PERGAMON

Scripta Materialia 47 (2002) 237–241

Scripta MATERIALIA

www.actamat-journals.com

# Phase-field simulation of hydride precipitation in bi-crystalline zirconium

X.Q. Ma [a], S.Q. Shi [a,*], C.H. Woo [a], L.Q. Chen [b]

[a] *Department of Mechanical Engineering, The Hong Kong Polytechnic University, Hung Hom, Kowloon, Hong Kong, China*
[b] *Department of Materials Science and Engineering, The Pennsylvania State University, University Park, PA 16802, USA*

Received 30 August 2001; accepted 6 March 2002

**Abstract**

The morphological evolution of γ-hydride precipitation and growth in a zirconium bi-crystal is simulated using a phase field kinetic model. The result shows the heterogeneous nucleation at the grain boundary. The likelihood of hydride growth across the grain boundary is discussed.


*Keywords:* Zirconium hydride; Bi-crystal; Computer simulation; Morphology evolution

## 1. Introduction

Zirconium and its alloys are important structural materials in nuclear industry. During services, these alloys pick up hydrogen from the environment. Above a certain level of hydrogen concentration, hydrides precipitate in the alloy. Because of the brittleness of the hydrides, the mechanical strength of the alloys is degraded [1], and fracture initiation at hydride precipitates may occur. It is believed that the critical conditions for fracture initiation at hydrides are controlled by the morphology and microstructure of hydride precipitates in the alloys [2–4].

The phase-field kinetic model is effective at describing the morphological evolution during phase transformation. It has been successfully applied to study of the morphology of second phase precipitation in many materials [5–9]. Recently, γ-hydride precipitation under an applied load in a zirconium single crystal was investigated [10] using the phase-field model based on the elasticity theory of Khachaturyan [11]. Most engineering materials are polycrystalline, and grain boundaries may play significant role in morphology evolution. Therefore, it is necessary to develop computational methods for polycrystalline materials. It should be noted that microstructure evolution during martensitic transformations in polycrystals has recently been studied using a phase-field model [12]. In this report, γ-hydride precipitation in a bi-crystalline zirconium is considered.

## 2. Model description

A coherent precipitate usually has a number of variants in terms of different crystallographically

* Corresponding author. Fax: +86-852-2365-4703.
*E-mail address:* mmsqshi@polyu.edu.hk (S.Q. Shi).

1359-6462/02/$ - see front matter 
PII: S1359-6462(02)00131-8

equivalent orientations. During the precipitation process, different variants are arranged in such a way that the free energy is minimized. The α-phase of zirconium has a hexagonal close-packed structure. The γ-hydride is formed as a result of either high rates of cooling or long-hold at room temperature, and has a face-centered tetragonal structure. The γ-hydrides appear needle-like with the axis along three $\langle 11\bar{2}0\rangle$ directions in a zirconium lattice [13]. In the phase-field kinetic model, the concentration of hydrogen in hydride precipitates and matrix is described by the conserved field variable $C(r,t)$, and the structural and orientation difference of hydride precipitates is represented by non-conservative field variables $\eta_p(r,t)$, also called long range order (LRO) parameters. In single crystal zirconium, three LRO parameters are required for γ-hydride, while in the case of a bi-crystal, a total of six LRO parameters are needed, with three in each grain.

According to thermodynamics, the equilibrium state of a multi-phase system corresponds to minimum free energy. The driving force for the temporal evolution of a multi-phase microstructure in single crystals consists of the following four major contributions: the reduction in chemical free energy, the increase in the total interfacial energy between different phases, the relaxation of the strain energy caused by the lattice mismatch between the matrix and precipitates, and the reduction in the interaction energy between the eigenstrain and external load. For bi-crystals, the free energy contribution due to the grain boundary should be included. The simulation will include all these five contributions to the total free energy in terms of the field variables $C(r,t)$ and $\eta_p(r,t)$.

The total chemical free energy of a multi-phase system may be expressed as [14]

$$F_c = \int_v \left[ f(C,\eta_p(r)) + \sum_{p=1}^{v} \frac{\alpha_p}{2} (\nabla \eta_p(r))^2 + \frac{\beta}{2} (\nabla C)^2 \right] \mathrm{d}^3 r \tag{1}$$

where α and β are gradient energy coefficients. The integration is performed over the entire system. The last two terms are related to the interfacial energy between different phases. The first term, $f(C,\eta_p)$, the local specific chemical free energy, is approximated using a Landau-type of free energy polynomial

$$\begin{aligned} f(C,\eta_p) = {} & \frac{A_1}{2}(C-C_1)^2 + \frac{A_2}{2}(C-C_2)\sum_p^v \eta_p^2 \\ & - \frac{A_3}{4}\sum_p^v \eta_p^4 + \frac{A_4}{6}\sum_p^v \eta_p^6 + A_5 \\ & \times \sum_{q\neq p}^{v} \eta_p^2\eta_q^2 + A_6 \sum_{p\neq q, p\neq r}^{v} \eta_p^4(\eta_q^2+\eta_r^2) \\ & + A_7 \sum_{p\neq q\neq r}^{v} \eta_p^2\eta_q^2\eta_r^2 \end{aligned} \tag{2}$$

where $v$ is the number of orientation variants, $C_1$ and $C_2$ are equilibrium concentrations of hydrogen in matrix and precipitate, respectively, and $A_1$–$A_7$ are phenomenological constants.

The elastic energy is caused by lattice mismatch between the precipitate and matrix. According to Khachaturyan's theory, elastic energy can be expressed as [11]

$$\begin{aligned} E_{\mathrm{el}} = {} & \frac{V}{2} C_{ijkl}\bar{\varepsilon}_{ij}\bar{\varepsilon}_{kl} - VC_{ijkl}\bar{\varepsilon}_{ij}\sum_p^v \varepsilon_{kl}^0(p)\overline{\eta_p^2(r)} \\ & + \frac{V}{2} C_{ijkl}\sum_p^v\sum_q^v \varepsilon_{ij}^0(p)\varepsilon_{kl}^0(q)\overline{\eta_p^2(r)\eta_q^2(r)} \\ & - \frac{1}{2}\sum_p^v\sum_q^v \int \frac{\mathrm{d}^3 g}{(2\pi)^3} B_{pq}(n)\{\eta_p^2(r)\}_g^* \\ & \times \{\eta_q^2(r)\}_g \end{aligned} \tag{3}$$

where $\overline{(\ldots)}$ represent the volume average of $(\ldots)$, $V$ is the total volume of the system, $C_{ijkl}$ is the elastic constant tensor, and $\eta_p$ is the normalized long range order parameter describing the $p$th variant. It is equal to ±1 in the precipitate and near zero in the matrix. $\varepsilon^0(p)$ is the stress-free transformation strain for the $p$th variant when $\eta_p(r) = \pm 1$. $\varepsilon_{ij}^0(r) = \sum_p \varepsilon_{ij}^0(p)\eta_p^2(r)$, which denote the local stress-free transformation strain. $B_{pq}(n) = n_i\sigma_{ij}(p)\Omega_{jk}(n)\sigma_{kl}(q)n_l$, where $\sigma_{ij} = C_{ijkl}\varepsilon_{kl}^0(p)$, and $\Omega_{jk}(n)$ is the reverse matrix of $\Omega_{jk}^{-1} = n_iC_{ijkl}n_l$. $\mathbf{g}$ and $\mathbf{n} = \mathbf{g}/\mathrm{g}$ are a reciprocal vector and its unit vector in reciprocal space, respectively. $\{\eta_q^2(r)\}_g$ is

the Fourier transform of $\eta_q^2(r)$, and $\{\eta_q^2(r)\}_g^*$ is the complex conjugate of $\{\eta_q^2(r)\}_g$. The first term in Eq. (3) is constant, related to the homogeneous strain. The second term represents the elastic coupling between the applied stress or strain and the local strain. The third and fourth terms are the relaxation energy corresponding to the local stress-free strain and equilibrium local displacement respectively. The last term describes the strain-induced interaction between finite elements of different variants $p$ and $q$ located at the coordinates $r$ and $r'$.

For a bi-crystal, we assume that the grain boundary energy has the form as suggested by Read and Shockley [15]: in the small angle regime ($\theta < 15°$), the grain boundary energy density increases with the orientation difference $\theta$ between the two grains:

$$E_b = E_0\theta(A - \ln\theta) \tag{4}$$

where $E_0$ and $A$ are constants, depending on the material. In the large angle regime ($\theta \geqslant 15°$), the grain boundary energy density is assumed to be constant. In addition, it was observed in TEM experiments that grain boundaries were often the nucleation sites for the hydride [13]. We assume that the nucleation energy of hydrides is lower at the grain boundary because of the existence of impurities and defects. Once hydrides are formed at the grain boundary, the grain boundary energy $E_b$ is minimized due to the replacement of part of the original grain boundary by hydride particles. Therefore, there is a stronger driving force at the grain boundary region for hydride formation as compared to the bulk, and this driving force is assumed to be proportional to $\eta_p^2$. To reflect this assumption, we add a free energy term only in the grain boundary region, i.e.,

$$E = E_b\left(1 - a\sum \eta_p^2(r,t)\right) \quad \text{(at grain boundary)} \tag{5}$$

where $a$ is a constant related to the system. In our simulation, we assume $a = 1$ because of the lack of experimental data. This is similar to a concept used to simulate the effect of random defects on phase transition temperature [16]. The grain boundary region was specified as a thin layer having a width of a few grid elements in our simulation.

In the phase-field model, the temporal evolution of the microstructure is determined by solving the time-dependent Ginzburg–Landau equations [14,17] for $\eta_p(r,t)$, and the Cahn–Hilliard diffusion equation [18] for $C(r,t)$, i.e.,

$$\frac{\partial\eta_p(r,t)}{\partial t} = -L_p\frac{\delta F}{\delta\eta_p(r,t)} + \zeta_p(r,t) \tag{6}$$

$$\frac{\partial C(r,t)}{\partial t} = M\nabla^2\frac{\delta F}{\delta C(r,t)} + \xi(r,t) \tag{7}$$

where $L$ and $M$ are kinetic coefficients characterizing structural relaxation and diffusional mobility, $F$ is the total free energy of the system, and $\zeta_p(r,t)$ and $\xi(r,t)$ are Langevin random noise terms which are related to fluctuations in the long range order parameter and composition respectively. The noise terms satisfy Gaussian distribution and meet the requirements of the fluctuation–dissipation theorem. Since the above equations are non-linear with respect to field variables, we solve them numerically using a semi-implicit Fourier spectral method [19].

## 3. Results and discussion

Our simulations were conducted in a $256 \times 256$ two-dimensional uniform grid, with the $c$-axis of Zr crystal normal to the grid. Parameters $A_1$–$A_4$ were obtained by fitting $f(C,\eta_p)$ to the free energy phase diagram of the Zr-hydrogen system, and $A_5$–$A_7$ were chosen to ensure only one $\eta_p$ near $\pm 1$ at the same spatial point. The parameters used in our simulation are given as follows: $A_1 = 60.0$, $A_2 = -20.0$, $A_3 = 10.0$, $A_4 = 3.5$, $A_5 = A_6 = A_7 = 0.6$ all in the unit of $10^7\ \mathrm{J\,m^{-3}}$, $E_0 = 4 \times 10^7\ \mathrm{J\,m^{-3}}$, $A = 2.5$, $\alpha_p = \beta = 3.5 \times 10^7\ \mathrm{J\,m^{-3}}$, $L_p = 0.4\ \mathrm{J^{-1}\,s^{-1}}$, $M = 0.4\ \mathrm{J^{-1}\,s^{-1}\,m^2}$. The elastic constants of zirconium are $C_{11} = 155.40$ GPa, $C_{12} = 68.03$ GPa, $C_{13} = 64.60$ GPa, $C_{33} = 172.51$ GPa, $C_{44} = 36.31$ GPa, and $C_{66} = 44.09$ GPa [20]. The constants $E_0$ and $A$ in Eq. (4) were chosen so that the energy of the grain boundary was in the order of $1\ \mathrm{J\,m^{-2}}$. At current time, the lack of experimental data in the

literature has prevented us from defining more realistic values for $E_0$, $A$, $\alpha$, $\beta$, and the kinetic constant $M$. In particular, $L$ and $M$ were chosen in these simulations to optimize computational speed. Therefore, our study in the current stage is a qualitative investigation, rather than a quantitative one. A reduced time $t^* = t/t_0$ was used in the simulation to represent qualitatively the "aging time", where $t_0$ is about $10^{-7}$ $J^{-1}\,L^{-1}$. For each iteration, the time step was $\Delta t^* = 0.0008$.

A hexagonal to tetragonal transformation of $\gamma$-hydride precipitate from a single crystalline zirconium generates three possible equivalent orientation variants. The stress-free transformation strains for the first orientation domain [21] are 5.70% ([0 0 0 1]), 0.551% ([1 1 $\bar{2}$ 0]), 5.64% ([1 $\bar{1}$ 0 0]), and the shear components are all zero. The strains for the other two orientations are obtained by rotating the first orientation domain by 60° and 120° about the $c$-axis, respectively. In this simulation, the grain boundary is a vertical thin column through the center of the field. In the left-hand grain, the [1 1 $\bar{2}$ 0] direction is along the horizontal axis, while in the right-hand crystal the [1 1 $\bar{2}$ 0] direction tilts an angle $\theta$ with respect to the horizontal axis. The initial value of $C_0(r,t)$ was set at 0.1, all $\eta_p(r,t)$ were zero, and the two noise terms in Eqs. (6) and (7) were turned on during the first 1000 time steps to mimic the local thermal fluctuations of $C(r,t)$ and $\eta_p(r,t)$.

Fig. 1 shows the nucleation and growth process of $\gamma$-hydride precipitate in a bi-crystal zirconium matrix. The orientation of the right-hand crystal is rotated by 20° with respect to the left-hand crystal. It can be seen from Fig. 1(a) that, after the nucleation process, the density of the hydride nuclei near the grain boundary is larger than that at other places. In Fig. 1(b), one can see that in the growth stage, these nuclei grow along habit planes at an angle of about 120° from each other. It is also shown that hydride precipitated in one grain may stop growing across the grain boundary.

To study the likelihood of hydride growing across grain boundary, we only turn on one set of LRO along the [1 1 $\bar{2}$ 0] direction. The result is shown in Fig. 2. One can see that some hydride particles stop growing at the grain boundary, while others seem to grow across the boundary. TEM

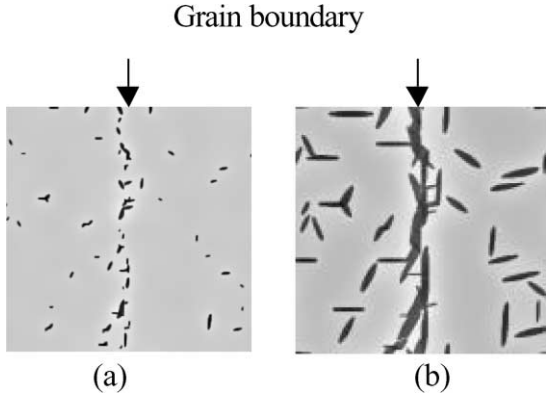


Fig. 1. Simulation results of $\gamma$-hydride precipitation in a bi-crystal zirconium at different precipitation times, $\theta = 20°$. (a) $t^* = 1500$, (b) $t^* = 4000$.

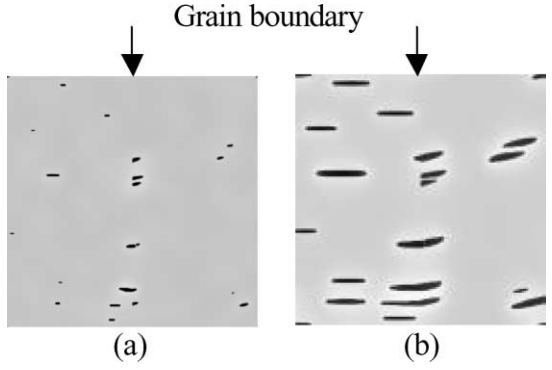


Fig. 2. Simulation results of $\gamma$-hydride precipitation in a bi-crystal zirconium with only one orientational variant in each grain, $\theta = 20°$. (a) $t^* = 1500$, (b) $t^* = 4000$.

observation by Bailey [13] showed similar hydride morphology at grain boundaries. Detailed examination of the simulation shows that hydrides usually stop growth at the grain boundary. However, if some small hydride nuclei already exist at the other side of the grain boundary, these nuclei may grow and connect with the hydrides in the neighbor grain.

Fig. 3 presents hydride morphology after 4000 time steps for different orientation differences between two crystals. In the situation of Fig. 3(a), the [1 1 $\bar{2}$ 0] directions of the grains on both sides of the boundary are along the horizontal axis. The orientation difference is zero. According to our assumption in Eqs. (4) and (5), the additional free

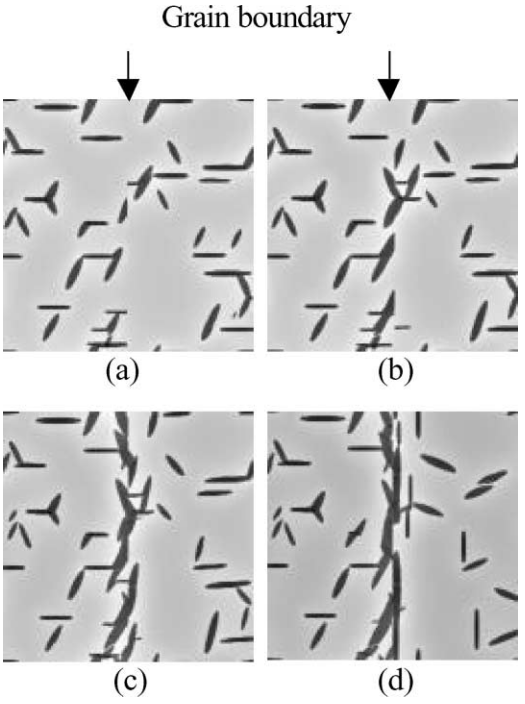


Fig. 3. Simulation results of γ-hydride precipitation in bi-crystal zirconium with different mis-orientation angles, $t^* = 4000$. (a) $\theta = 0°$; (b) $\theta = 5°$; (c) $\theta = 10°$; (d) $\theta = 30°$.

energy at the grain boundary is zero for this case, therefore there is no additional driving force at the grain boundary. Fig. 3(a)–(d) together with Fig. 1(b) show that the density of hydride precipitated at the grain boundary increases with the orientation difference between the crystals at the range of small angles, while remaining constant for the large angles, a natural result of our model.

## 4. Conclusions

- By adopting a total of six LRO with three LRO in each grain, the hydride precipitation process in a bi-crystal system has been simulated.
- The simulation result shows that the nucleation density of the hydride at the grain boundary increases as compared to the bulk under the assumption of Eq. (5).
- The hydride morphology obtained from the simulations is similar to that obtained from TEM observation.

## Acknowledgements

This work was supported by grants from the Research Grants Council of Hong Kong (B-Q411) for Shi and Woo, from The Hong Kong Polytechnic University (G-V851) for Ma, and from the US National Science Foundation (DMR 96-33719) for Chen.

## References

[1] Simpson LA, Cann CD. J Nucl Mater 1979;87:302.
[2] Shi SQ, Puls MP. In: Thompson AW, Moody NR, editors. Hydrogen Effects in Materials. New York: TMS; 1996. p. 611.
[3] Shi SQ, Puls MP. J Nucl Mater 1994;208:232.
[4] Shi SQ, Puls MP, Sagat S. J Nucl Mater 1994;208:243.
[5] Chen LQ, Wang YZ, Khachaturyan AG. Philos Mag Lett 1992;65:15.
[6] Wang YZ, Wang HY, Chen LQ, Khachaturyan AG. J Am Ceram Soc 1995;78:657.
[7] Fan D, Chen LQ. J Am Ceram Soc 1995;78:769.
[8] Wang Y, Khachaturyan AG. Acta Mater 1997;45:759.
[9] Li DY, Chen LQ. Acta Mater 1998;46:2573.
[10] Ma XQ, Shi SQ, Woo CH, Chen LQ. Comp Mater Sci 2002;23:283.
[11] Khachaturyan AG. Theory of Structural Transformations in Solids. New York: John Wiley & Sons; 1983.
[12] Artemev A, Wang Y, Khachaturyan AG. Acta Mater 2000;48:2503.
[13] Bailey JE. Acta Metal 1963;11:267.
[14] Wang Y, Chen LQ, Khachaturyan AG. J Am Ceram Soc 1993;76:3029.
[15] Read WT, Shockley W. Phys Rev 1950;78:275.
[16] Semenovskaya S, Khachaturyan AG. Acta Mater 1997;45:4367.
[17] Cahn JW, Hilliard JE. J Chem Phys 1958;28:258.
[18] Allen SM, Cahn JW. Acta Metal 1979;27:1085.
[19] Chen LQ, Shen J. Comput Phys Commun 1998;108:147.
[20] Lgarashi M. Phil Mag B 1991;63:603.
[21] Carpenter GJC. J Nucl Mater 1973;48:264.